EPJ Plus

EPJ.org
your physics journal

Eur. Phys. J. Plus (2012) **127**: 124 DOI 10.1140/epjp/i2012-12124-9

Further evidence for low-energy protonium production in vacuum

E. Lodi Rizzini, L. Venturelli, N. Zurlo, M. Charlton, C. Amsler, G. Bonomi, C. Canali, C. Carraro, A. Fontana, P. Genova, R. Hayano, L.V. Jorgensen, A. Kellerbauer, V. Lagomarsino, R. Landua, M. Macrí, G. Manuzio, P. Montagna, C. Regenfus, A. Rotondi, G. Testera, A. Variola and D.P. van der Werf

Società Italiana di Fisica

Springer

Eur. Phys. J. Plus (2012) **127**: 124
DOI 10.1140/epjp/i2012-12124-9

THE EUROPEAN PHYSICAL JOURNAL PLUS

Regular Article

Further evidence for low-energy protonium production in vacuum

E. Lodi Rizzini[1,2], L. Venturelli[1,2], N. Zurlo[1,2], M. Charlton[3], C. Amsler[4,a], G. Bonomi[5,6], C. Canali[4], C. Carraro[7,8], A. Fontana[6], P. Genova[6,9], R. Hayano[10], L.V. Jørgensen[3,b], A. Kellerbauer[11,c], V. Lagomarsino[7,8], R. Landua[11], M. Macrí[7], G. Manuzio[7,8], P. Montagna[6,9], C. Regenfus[4], A. Rotondi[6,9], G. Testera[7], A. Variola[7,d], and D.P. van der Werf[3]

[1] Dipartimento di Chimica e Fisica per l'Ingegneria e per i Materiali, Università di Brescia, 25133 Brescia, Italy
[2] Istituto Nazionale di Fisica Nucleare, Gruppo Collegato di Brescia, 25133 Brescia, Italy
[3] Department of Physics, College of Science, Swansea University, Singleton Park, Swansea SA2 8PP, UK
[4] Physik-Institut, Zürich University, 8057 Zürich, Switzerland
[5] Dipartimento di Ingegneria Meccanica, Università di Brescia, 25123 Brescia, Italy
[6] Istituto Nazionale di Fisica Nucleare, Sezione di Pavia, 27100 Pavia, Italy
[7] Istituto Nazionale di Fisica Nucleare, Sezione di Genova, 16146 Genova, Italy
[8] Dipartimento di Fisica, Università di Genova, 16146 Genova, Italy
[9] Dipartimento di Fisica Nucleare e Teorica, Università di Pavia, 27100 Pavia, Italy
[10] Department of Physics, University of Tokyo, Tokyo 113-0033, Japan
[11] Physics Department, CERN, 1211 Geneva 23, Switzerland

Received: 3 September 2012 / Revised: 20 September 2012
Published online: 10 October 2012

Abstract. We describe an experiment performed in the ATHENA apparatus in which there is evidence that the antiproton-proton bound state, protonium, has been produced at very low energies in vacuum following the interaction of cold antiprotons with a trapped cloud of molecular hydrogen ions. The latter were confined in a centrifugally separated belt outside a positron plasma used for antihydrogen formation. Studies have been performed at low positron plasma temperatures in which the protonium annihilation signal has been identified along with that from antihydrogen, and we discuss how their contributions can be disentangled. With the positron plasma heated to around 10000 K the ions become distributed in the positrons, and the majority of the annihilation signal can be explained in terms of protonium formation, as antihydrogen creation is heavily suppressed. In this case we compare the observed protonium formation rate with expectations from theory and find reasonable accord, when experimental systematics are taken into account. The effect on the annihilation signals of the passage of an electron current through a pre-loaded positron plasma has been studied in detail, and the results are presented here for the first time.

1 Introduction and motivation

Spectroscopic studies of few-body bound states have produced some of the most precise determinations of physical quantities. Such measurements provide powerful tests of our understanding of the laws of physics, often via stringent comparisons with theory. The most well-known frequencies are those for the $1S$-$2S$ two-photon Doppler-free transition [1] and the so-called maser transition for the ground-state hyperfine splitting [2], in atomic hydrogen. The former is known to an accuracy of just above 4 parts in 10^{15}, or to an absolute precision of 10 Hz in 2466 THz. Unfortunately, in this case, this impressive achievement cannot be matched by theory due to uncertainties in the properties of the proton: see, *e.g.*, [3,4].

The attractiveness of laser spectroscopy of hydrogen derives from the metastable nature of the $2S$ level, which guarantees a natural linewidth of around 1 Hz. Despite the lack of theoretical comparative input, there is much

[a] *Present Address*: Albert Einstein Center for Fundamental Physics, University of Bern, 3012 Bern, Switzerland
[b] *Present Address*: BE-Department, CERN, 1211 Geneva 23, Switzerland
[c] *Present Address*: Max Planck Institute for Nuclear Physics, Saupfercheckweg 1, 69117 Heidelberg, Germany
[d] *Present Address*: L.A.L. (Laboratoire de l'Accélérateur Linéaire), Université Paris-Sud, Bâtiment 209a, F-91898 Orsay Cedex, France

current interest in this area due to the production [5,6], and the recent demonstration of trapping [7–10], of low-energy antihydrogen, since comparisons of the transitions in hydrogen and antihydrogen may offer tests of CPT symmetry. Experimental studies to realise high-precision microwave spectroscopy of the hyperfine transitions of ground-state antihydrogen are in progress, both with magnetically trapped antihydrogen [7,8], in which the first resonant quantum transition in the antiatom has recently been observed [11], and with a spin-polarised beam [12].

Other few-body systems which have been studied using laser spectroscopy are positronium (e^+e^-) (see, *e.g.*, [13,14] for the most recent work), muonium (μ^+e^-) [15–17] and antiprotonic helium ($\overline{p}\mathrm{He}^+$) (see [18–20] for recent reviews and progress). These systems provide complementary information to the hydrogen work, for instance in the form of mass ratios and can, when combined with other measurements (such as precision charge-to-mass determinations from Penning trap experiments) yield further information, for instance on CPT. This information is useful, despite the fact that, ultimately, the precision with which spectroscopic lines may be resolved is limited by bandwidth arising either from annihilation or decay.

Protonium ($\overline{p}p$), sometimes known as antiprotonic hydrogen, is the quasi-stable antiproton ($\overline{p}$)-proton bound system. Recall, from the Bohr formula, that the binding energies are proportional to the reduced mass of the system. Thus, over the years, this entity was studied following the stopping of antiprotons in dense gaseous targets (typically hydrogen) using X-ray spectroscopy of the inner shell cascades (see, *e.g.*, [21,22]). Note that the excited states formed during the cascades were rapidly quenched due to Stark collisions [23,24].

More recently a radically different method of protonium production has been described [25] which involved interactions of trapped, cold antiprotons with molecular hydrogen ions (H_2^+) via the reaction,

$$\overline{p} + \mathrm{H}_2^+ \rightarrow \overline{p}p(n,l) + \mathrm{H}. \tag{1}$$

This was achieved using the nested Penning trap deployed by ATHENA for the first production of low-energy antihydrogen [5]. A crucial feature was the serendipitous trapping of around 10^4–10^5 H_2^+ ions along with the positron cloud used for antihydrogen formation.

The ATHENA study found that the protonium atoms were created almost at rest, and in such a way that could easily be scaled up, with more trapped antiprotons and hydrogen ions, to facilitate further investigation of the properties of protonium. In particular, it was deduced (as will be summarised in sect. 3.2) that the protonium was liberated in an excited state, estimated to be with a principal quantum number around $n = 68$. This can allow access to energy levels and transitions using laser spectroscopy. Thus, we may look forward to new, high-precision, studies of protonium similar to those for $\overline{p}\mathrm{He}^+$ [18–20], which in some cases have now reached resolutions in the region of a few parts in 10^9.

Further studies of protonium are likely to be of benefit for two major reasons; as tests of CPT in the baryon sector and as stringent tests of two-body bound-state physics. For instance, it is likely that improvements can be made in comparisons of the charges and masses of the proton and the antiproton, which currently stand at precisions of around parts in 10^9 [20,26].

In this communication we elaborate on the findings discussed in [25]. Data are presented on observations in which removal of the H_2^+ ions eliminates the protonium signal, and we also provide a detailed examination of the radial and axial distributions of the protonium annihilations.

2 Experimental details

The experiments took place at CERN's Antiproton Decelerator (AD), which is a unique facility providing 200 ns long pulses comprised of around 2×10^7 antiprotons, with a kinetic energy close to 5.3 MeV, every 90 s or so. The antiprotons were delivered to the ATHENA apparatus (an overview of which is given in fig. 1) which contained a multi-electrode cylindrical Penning trap, 2.5 cm in diameter and $\sim$ 90 cm in length immersed in an axial magnetic field of 3 T. The electrodes of the trap were held in thermal contact with a cryogenic bath such that they were typically cooled to a temperature of around 15 K. A schematic of the central portion of the trap which was used for the ATHENA experiments is shown in fig. 2.

A small fraction (typically one per mille) of the antiprotons were dynamically captured in the trap, following energy degradation in a thin foil. Only those antiprotons with kinetic energies below about 5 keV could be caught using a pulsed gate on a Penning-type trap [28–30]. Once held in the trap the antiprotons passed to-and-fro through a pre-loaded cloud of about 10^8 electrons, which had cooled towards the trap ambient temperature via the emission of synchrotron radiation. The antiprotons coupled efficiently to the electrons via the Coulomb interaction and were sympathetically cooled to the electron temperature within a few seconds. Further details can be found elsewhere [27]. We note here that ATHENA experimented with more than one method of transferring electrons into the nested well arrangement. In one scenario the electron trap was filled by passing them through the positron cloud, which had been pre-loaded. The effect of this so-called electrons-through-positrons (ETP) procedure, which has not hitherto been described, will be one of the results presented here.

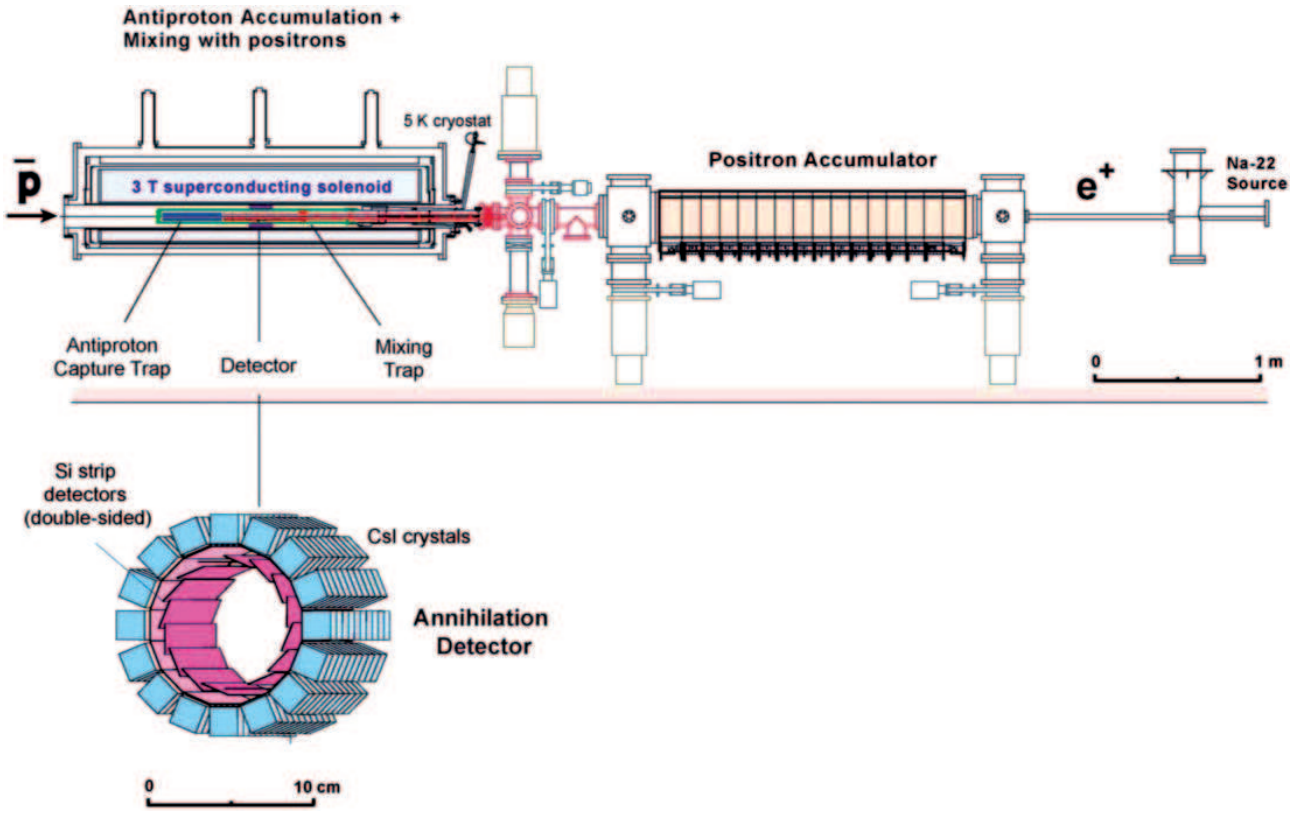

Fig. 1. Overview of the ATHENA apparatus showing the positron accumulator, the antiproton trap and the mixing region used to create antihydrogen and protonium. A detector capable of registering both $\overline{p}$ and e^+ annihilations was located around the mixing region and is shown in the sketch below the main apparatus [27].

Positrons for use in the ATHENA experiments were accumulated in a separate apparatus, shown schematically on the right of fig. 1, which used buffer gas cooling to enable trapping and storing of the antiparticles in a Penning-Malmberg trap. The positrons were derived from a ^{22}Na source, and around 0.5% of these were released into vacuum with a few eV of kinetic energy following moderation using a thin solid neon film. The physics of positron moderation is well understood (see, *e.g.*, [31]) and the use of solid neon as an efficient means of producing a low-energy beam is long established [32–34]. A 3-stage buffer gas positron accumulator, as pioneered by the UCSD group of Surko and co-workers [35,36], was employed [27,37] to collect about 200 million positrons in a 2–3 minute period. These were then transferred to the main ATHENA magnet, as described elsewhere [38], where typically 75 million were available for further experimentation by ATHENA. Once inside the 3 T magnetic field, the positrons, like the electrons used for $\overline{p}$ cooling, rapidly reached a temperature close to that of the ambient, which was around 15 K.

Non-destructive diagnostics were developed by ATHENA using plasma oscillation modes to deduce the total number of particles in the plasma, and its radius and aspect ratio [39,40]. The plasma was presumed, following [41,42], to form a spheroid (though this was not tested directly). Many antihydrogen experiments were performed by mixing clouds of antiprotons and positrons under ambient trap conditions; so-called cold mixing (CM). Furthermore, the temperature increase of the positrons could be monitored following the application of a radio frequency excitation signal to one of the trap electrodes in the vicinity of the plasma. Using this heating the temperature of the positron plasma could be increased as required and it was found that a convenient background signal for antihydrogen formation could be found by heating the positron plasma to several thousand K [43]. In this so-called hot mixing (HM) scenario antihydrogen formation was almost entirely suppressed.

During the course of ATHENA experimentation it was estimated [25] that the trap contained typically 10^4–10^5 H_2^+ ions, under conditions of residual gas pressure of 10^{-12} mbar, with the trap electrodes held at a temperature of 15 K. These ions were not introduced deliberately, but probably arose during transfer of the positrons into the main magnet. This procedure [38] involved slowly squeezing the positrons into the mixing region over time periods of the order of 25 s, allowing them the opportunity to collide with H_2 molecules which formed part of the residual gas in the vacuum chamber. The kinetic energy of the positrons during transfer was typically 25 eV such that the production of H_2^+ ions via positronium formation and direct ionization would both have been feasible [44–46]. Ions may also have

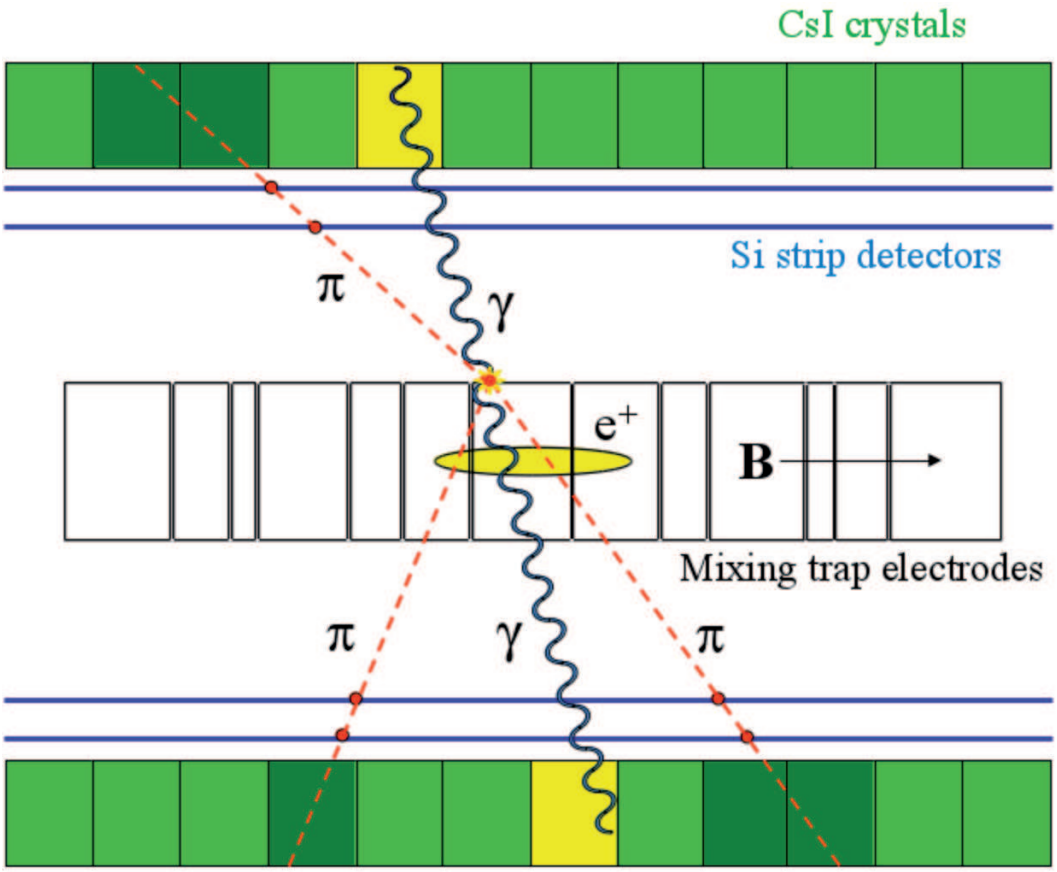

Fig. 2. Schematic illustration of the central portion of the trap and detector. The cylindrical electrodes of the mixing trap are aligned with the axis of a 3 T solenoid (not shown). The silicon strip detector (for charged pion detection) and the CsI scintillators (to register the 511 keV γ-rays from e^+ annihilation) are shown surrounding the traps as the horizontal lines and arrays of blocks, respectively. A schematic of an antihydrogen annihilation event is shown.

been produced during $\overline{p}$ loading, as has previously been deduced by the ATRAP collaboration [47]. We note that the number of H_2^+ ions should be independent of the temperature of the positron plasma, and is thus expected to be similar for the CM and HM cases. This is because the positron loading technique was identical for both cases and clearly occurred before the positron temperature was raised for the HM experiments.

The ATHENA mixing trap was surrounded by a position sensitive detector which could allow antihydrogen annihilation on the electrode walls of the trap to be monitored. The detector, which is shown schematically in figs. 1 and 2, has been described in detail elsewhere [27,48]. It consisted of two cylindrical layers of 16 double-sided silicon strip detectors surrounded by 192 (16×12) CsI scintillators. The latter were used to detect the back-to-back 511 keV gamma rays emitted in positron annihilation, whilst the silicon detectors were used to reconstruct the antiproton annihilation vertices by registering the passage of charged pions emitted in such events. Space constraints in the apparatus meant that only two layers of silicon counter could be used, such that the ATHENA detector was unable to reconstruct the curved trajectories of the charged pions in the 3 T magnetic field. This was the main cause of the uncertainties (standard deviations) in the vertex determination of $\sigma_z = 1.8$ mm and $\sigma_{x,y} = 3.5$ mm.

Full antihydrogen events consisted of both types of annihilation recorded in spatial and temporal coincidence [5,27]. These events were typically plotted as a function of the cosine of the angle between the pair of gamma-ray events (*i.e.* $\cos(\theta_{\gamma\gamma})$) as seen from the location of the $\overline{p}$ annihilation vertex, the so-called opening angle plots. A fully reconstructed antihydrogen annihilation event would contribute to such a plot at, or near, $\cos(\theta_{\gamma\gamma}) = -1$, and examples of data with a feature at this angle are discussed below. However, it was also found [43] that antihydrogen signals could be isolated by monitoring the $\overline{p}$ annihilation vertices alone during the relevant mixing period. Analysis of the spatial distribution of these vertices will be discussed below. Though the ATHENA CM vertex data were predominantly due to antihydrogen annihilations, there was also a clear component resulting from protonium formation and annihilation. The latter, which is the subject of this communication, was present for both CM and HM experiments.

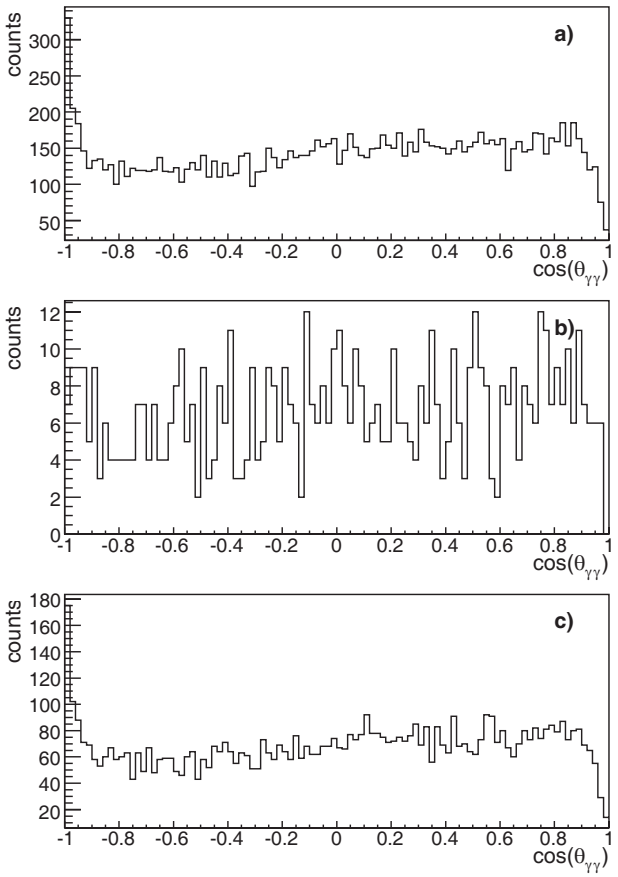

Fig. 3. Opening angle plots for the (a) ETP, (b) HM and (c) CM data sets. Only the data for which $r > 1\,\mathrm{cm}$ (see text) have been selected here to reduce the contribution from protonium annihilations, which tend to be near-axis.

3 Data, analysis and discussion

3.1 Data and analysis

In order to set the scene for the analysis of the data, we present in fig. 3 the opening angle plots for data taken in ETP, HM and CM conditions. The vivid differences between these plots in the region of $\cos(\theta_{\gamma\gamma}) = -1$ highlights the essentials of the analysis to be presented below. The peak characteristic of antihydrogen annihilation is evident in the CM and ETP samples. We find that in the latter, as will be argued below, we can attribute all of the annihilation events to antihydrogen. The peak is absent in the HM case, indicating a dearth of antihydrogen formation. The origin of the annihilation signals in this case is one of the topics discussed herein, and is predominantly a result of protonium formation and its annihilation in flight.

The following analysis presents data for the conditions for which the majority of the ATHENA data were taken, namely the standard CM case where the positron density, n_e, was in the range $5\text{–}8 \times 10^8\,\mathrm{cm}^{-3}$ and the HM case at a similar density, but with the positron temperature, T_e, raised to $\sim 10^4\,\mathrm{K}$.

The $\overline{p}$ annihilation vertices could be sorted according to their radial (r, the distance from the trap axis) and axial (or longitudinal, z) positions and, if appropriate, the time they occurred after the start of the $\overline{p}$-e^+ mixing to aid, for instance, in the separation of protonium annihilations from those due to antihydrogen. The use of such data cuts will be discussed as necessary below. Note, as mentioned in sect. 2, the vertex distributions are broadened by detector resolution.

For reasons connected to the efficient production of antihydrogen in ATHENA, several different mechanisms were used to load electrons into the main ATHENA magnet. (Recall that, as described in sect. 2, the electrons were used to cool the antiprotons towards the ambient temperature of the trap using a well-established technique [29,30].) In particular, data were obtained under CM conditions when the electrons were loaded, before positron-antiproton mixing, by passing them through the positron plasma (ETP). This mode of loading caused the positron plasma to expand such that the density was reduced to values between $0.5\text{–}1.6 \times 10^8\,\mathrm{cm}^{-3}$. Figure 4(a) shows the resulting r-z scatter

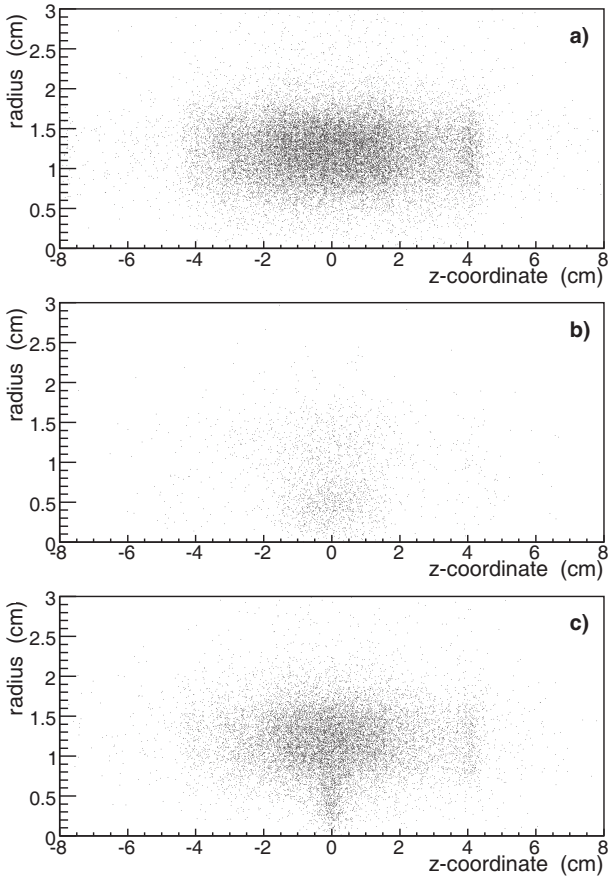

Fig. 4. Scatter plots in the r-z plane for the annihilation vertices for the (a) ETP, (b) HM and (c) CM data sets.

plot, whilst figs. 5(a) and (d) give radial distributions and figs. 6(a) and (d) the corresponding axial distributions for this ETP case, broken down into two portions according to their respective z- (fig. 5) or r- (fig. 6) positions.

The events in the scatter and radial plots, figs. 4(a) and 5(a) and (d), are centred close to the radius of the trap electrode (1.25 cm), whereas the axial distributions given in fig. 6(a) and (d) are spread across a wide range of z. These are typical of antihydrogen annihilations [49]. Furthermore, the shape of the axial distributions for data cuts for which $r > 0.5$ cm and, for the few events present at $r < 0.5$ cm (figs. 6(d) and (a), respectively) are similar, and the peaked distribution centred around $z = 0$ for $r < 0.5$ cm, which is characteristic of protonium annihilation in flight (see [25] and fig. 6(c)), is absent. Thus, these data seem to be an example of a pure antihydrogen signal and will be used as a reference for comparison with the distributions when protonium is also present.

It is important to note here that the radial ETP vertex distribution is identical to that arising from antiproton-only annihilation on the walls of the Penning trap. The latter was obtained in dedicated experiments without the presence of positrons and, therefore, also in the absence of H_2^+ ions. In addition, these distributions are in accord with a full Monte Carlo simulation of antiproton annihilation on the trap walls (see figs. 5(a) and (d)). These simulations, which are intended to mimic the $\overline{p}$ vertices resulting from antihydrogen annihilation on the wall of the trap, have been used to extract the fraction of on-wall annihilations from data also containing protonium annihilations (see table 1 and fig. 5). The simulated antihydrogen events were generated by means of the ATHENA Monte Carlo program and processed by the same reconstruction program used to determine the annihilation vertices of the real data [27]. In the Monte Carlo program, which is based upon the CERN GEANT3 package, a full description of the geometry of the ATHENA apparatus, including the efficiency of the detectors, is implemented. A phase space event generator for the $\overline{p}$-p or e^+-e^- annihilations has been specifically written in order to simulate the antihydrogen annihilation events. Actually, when antihydrogen strikes the wall of the Penning trap, the annihilation of the antiproton occurs on a nucleus. In this case the use of the branching ratios arising solely from $\overline{p}$-p annihilations [50] instead of these parameters for the antiproton-nucleus system, and which are poorly known, can introduce a bias, in particular via an overestimation of the number of neutral pions produced in the simulation [27]. However, for the present purposes this effect is negligible, as we have only used the Monte Carlo program to determine the radial distribution of the reconstructed vertices from antihydrogen annihilation.

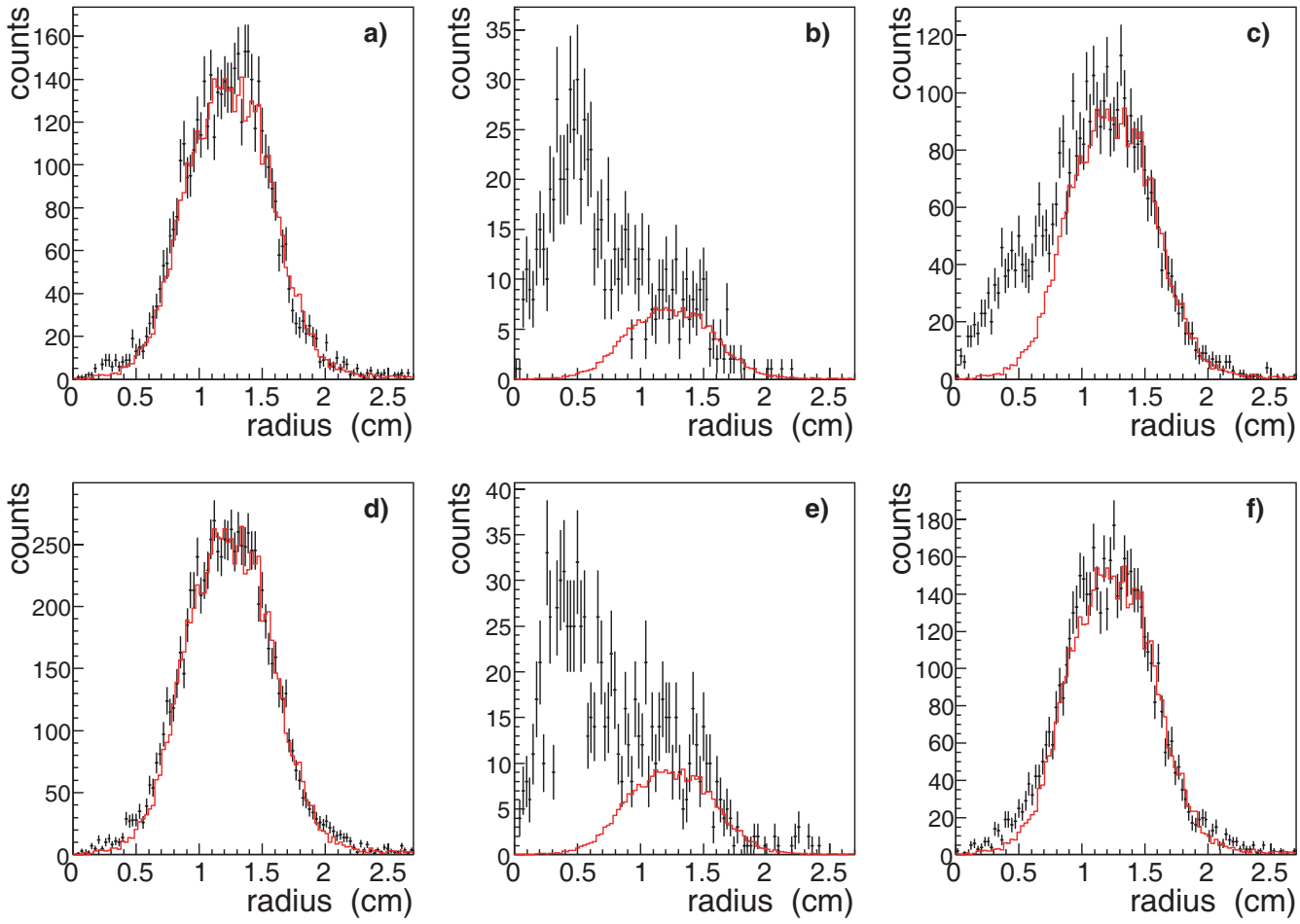

Fig. 5. Radial annihilation distributions for the antiproton annihilation vertices for the ETP (a) and (d), HM (b) and (e) and CM (c) and (f) data sets separated into events for which the axial positions are $|z| < 0.5\,\text{cm}$ ((a)-(c)) and $0.5 < |z| < 1.5\,\text{cm}$ ((d)–(f)). Shown in red is the Monte Carlo simulation (see text for details) for antiproton annihilation on the electrode wall fitted in each case to the higher radius (beyond $r = 1.25\,\text{cm}$) portion of the data.

There are other noteworthy features of the ETP data. It is evident from the scatter plot and the axial distributions referred to above that clusters of events are found at various axial positions (*e.g.*, the bands of events centred at $z = +\,4\,\text{cm}$; see also figs. 6(d) and (f)). Such "hot spots" have been seen previously in ATHENA [51] (though not under typical CM conditions) and they are located close to the gaps between the Penning trap electrodes where the electric fields are highest. A similar phenomenon has also been noted recently by the ALPHA collaboration [52] where it was attributed to antiproton annihilation following field ionization of weakly bound states of antihydrogen formed via the three-body process (see, *e.g.*, [53] for a discussion of the physics of antihydrogen formation). Such ionization may occur near the electrode gaps where the electric field is highest, and is a likely cause of these features in ATHENA. We note that they cannot be caused by the annihilation on the wall of $\overline{p}p$ following field ionization as this entity is bound by several eV and cannot be broken up by any of the fields present in the experiment.

During its many CM antihydrogen experiments, the positron density, n_e, used by ATHENA changed due to different operating conditions of the positron accumulator and to variations in positron loading and manipulation. However, our discussion of CM concentrates, as mentioned above, on the density range $5\text{–}8 \times 10^8\,\text{cm}^{-3}$ that received the most attention and for which the largest data sets exist.

Before embarking on this, however, it is worthwhile to recall the state of thermal equilibrium of a plasma which contains species of the same sign of charge, but different masses. We note that the radial self electric field, $E = n_e e r/2\epsilon_0$, of a long, spheroidal plasma (such as those used in this study) when combined with the axial magnetic field B, leads to a tangential velocity of the plasma, which at its surface (at r_p) is given by $v_{tang} = n_e e r_p/2\epsilon_0 B$. Thus, the positron plasma will experience $\mathbf{E}\times\mathbf{B}$ rotation around the magnetic field lines with a constant angular frequency of $n_e e/2\epsilon_0 B$. Any ions present in the plasma will, in equilibrium, co-rotate with this frequency, and as a result will centrifugally separate from the positrons [54,55]. The effects of centrifugal separation have been observed in experiments involving cooled Be^+-ion

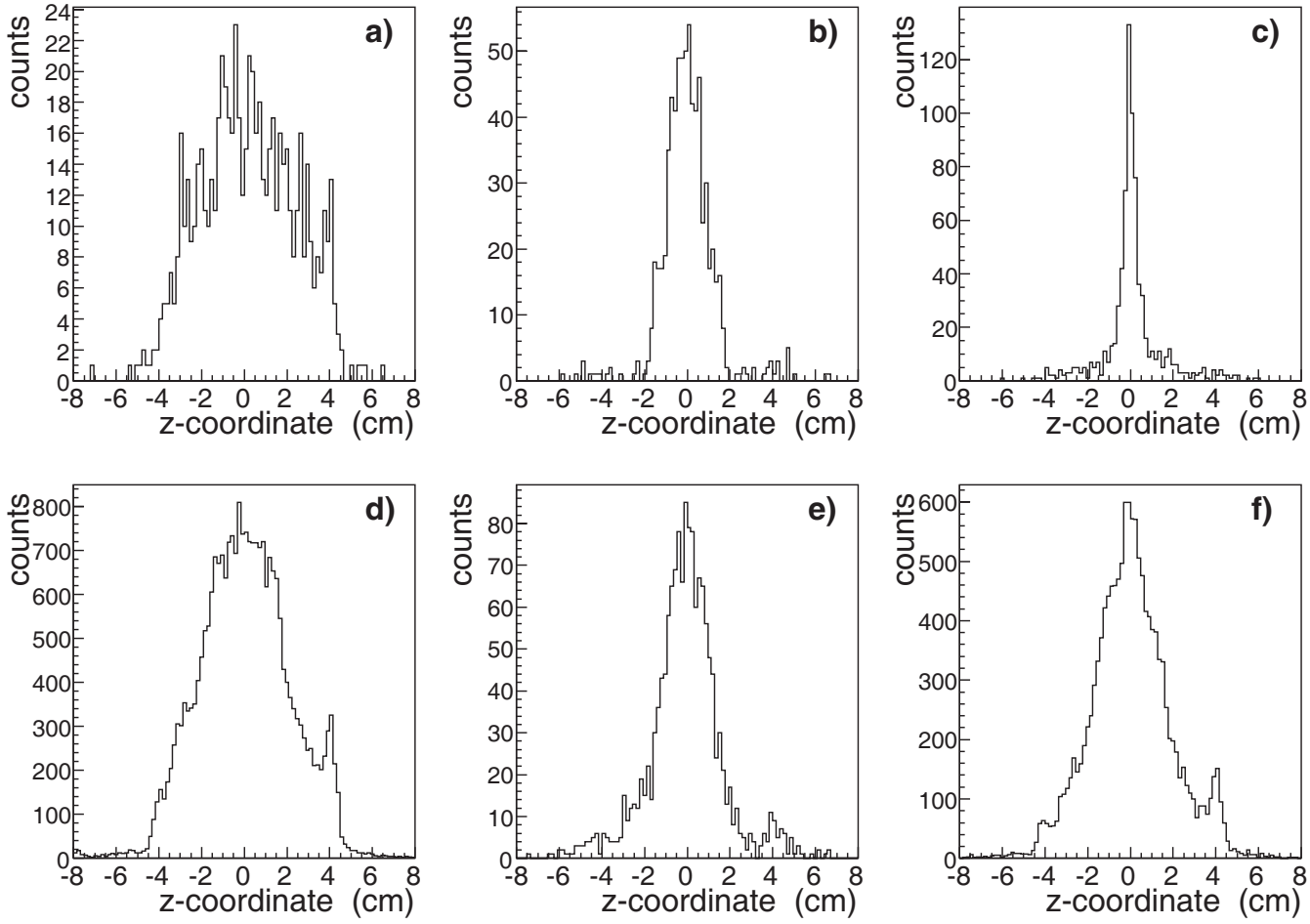

Fig. 6. Vertex axial distributions for ETP (a) and (d), HM (b) and (e) and CM (c) and (f) data sets. Boxes (a)-(c) correspond to data for which $r < 0.5\,\mathrm{cm}$, with (d)-(f) for $r > 0.5\,\mathrm{cm}$.

systems [56,57], and also in the Be^+-positron case [58]. More recently, centrifugally separated electron-antiproton systems have been observed [59,60]. In the ALPHA experiment [59] aspects of the dynamics of the separation were studied for the first time. The ions will also migrate towards the minimum in the potential, which is located at the centre of the positron cloud. Thus, the ions, when cold (see below), will form an equatorial belt around the centre of the positron plasma.

Both antiproton experiments [59,60] point out that the condition for which separation occurs, irrespective of the sign of the charge of the plasma and ions, is when $v_{tang} = v_{th}$, with the latter the thermal speed. Using $v_{th} = (2k_B T_e/m)^{1/2}$ it can be shown that the value of T_e at which centrifugal separation should be possible, denoted by T_{sep}, is given by,

$$T_{sep} = \frac{me^2}{8\epsilon_0^2 k_B}\left(\frac{n_e r_p}{B}\right)^2. \tag{2}$$

Inserting values for the H_2^+ ion at a magnetic field of 3 T reveals that $T_{sep} \sim 10(n_e r_p)^2$, with n_e in units of $10^8\,\mathrm{cm}^{-3}$ and r_p in mm. Thus, the values of T_{sep} for both the CM and HM cases ($n_e \sim$ 5-8 $\times\, 10^8\,\mathrm{cm}^{-3}$ and $r_p \sim 1\,\mathrm{mm}$) is around 250–640 K, or approximately 22–56 meV. Thus, although no absolute T_e diagnostic was available to ATHENA, $T_{sep} \gg 15\,\mathrm{K}$, the temperature of the trap electrodes, and the localization of the protonium events in the CM case [25] indicates that the positron temperature is much lower than T_{sep}. On the contrary, for HM $T_e \gg T_{sep}$.

Recent simulation work [61] has shown that the antiproton-positron dynamics in dense ($\sim 10^9\,\mathrm{cm}^{-3}$) positron clouds is very complex and is dominated by repeated cycles of antihydrogen formation and break-up. This has the effect of driving the antiprotons radially outwards such that they tend to form antihydrogen close to the edge of the plasma. The result is a lowering of the antihydrogen binding energy, such that it is more likely to be field ionized near the edge of the plasma, where the electric fields are strongest (excluding those fields very close to the electrode walls), resulting in the development of an antiproton population just outside the positron plasma. A similar observation relating to

Table 1. The fraction of the events (in %), F_c, that cannot be attributed to wall annihilations for the ETP, CM and HM ($T_e \sim 10000\,\mathrm{K}$) samples broken down into the three axial regions, $|z| < 0.5\,\mathrm{cm}$, $0.5 < |z| < 1.5\,\mathrm{cm}$ and the Penning trap side wells with $2.5 < |z| < 3.5\,\mathrm{cm}$, denoted as R_1, R_2 and R_3, respectively

Experimental Case	$F_c(R_1)$	$F_c(R_2)$	$F_c(R_3)$
ETP sample	5.2 ± 1.5	4.7 ± 1.2	7.7 ± 1.7
Hot Mixing	70.1 ± 4.4	68.8 ± 4.0	17 ± 11
Cold Mixing	23.9 ± 1.7	7.8 ± 1.4	5.8 ± 2.7

the antihydrogen-mediated radial transport of antiprotons was recently made by the ALPHA antihydrogen trapping experiment in a study of the dynamics of antihydrogen formation in their octupolar neutral atom trap [62]. Since, under CM conditions, the H_2^+ ions occupy an equatorial belt outside the positrons, the aforementioned antihydrogen formation and break-up cycles may act in such a way as to promote the production of protonium.

We have also examined the behaviour of the radial yields from fig. 5, broken down, as in the figure into the two axial regions $|z| < 0.5\,\mathrm{cm}$ and $0.5 < |z| < 1.5\,\mathrm{cm}$, with the addition of a third region at larger $|z|$ ($2.5 < |z| < 3.5$) cm. (The latter is outside the positrons in the so-called side wells of the Penning trap used to confine the plasma.) To do this we have used the results of the Monte Carlo simulations shown in the figure which, as described above, correspond only to annihilation events on the electrode walls. The parameter F_c, which is the fraction of the reconstructed vertices which cannot be attributed to wall annihilations was derived as the difference in the counts between the experimental distribution and the fitted Monte Carlo component divided by the total number of entries in the experimental case. The results are presented in table 1 where we note that the lower the value of F_c, the higher the antihydrogen yield.

The ETP sample has the lowest F_c and is thought to be entirely due to antihydrogen formation and annihilation. The small ($\sim 5\%$) fraction of events which cannot be directly attributed to wall annihilations may, however, be the result of a deficiency of the Monte Carlo programme to simulate the poorly reconstructed vertices, or the result of annihilations on the neutral residual gas inside the trap (see below). There is no dependence of F_c on z, as expected for antihydrogen events. By contrast, the HM sample contains $\sim 70\%$ non-wall annihilation events, which is consistent with protonium formation and annihilation, since this sample should have a very low antihydrogen yield. Again F_c does not depend upon z, indicating that the source of the annihilation is uniformly distributed in the axial direction, at least in the vicinity of the positron plasma.

Intermediate between these two is the CM sample which for $|z| < 0.5\,\mathrm{cm}$ has $\sim 24\%$ of its events which cannot be attributed to wall annihilations and these are clearly visible in the low-r bulge in fig. 5(c). In this case, however, F_c falls to $\sim 8\%$ and lower at larger values of $|z|$ (see fig. 5(f)) indicating that antihydrogen is more prevalent in this sample of events. This is caused by the aforementioned localization of the ion cloud around the positron plasma. Protonium formation (and annihilation) is localized in this case, mainly to the region for which $|z| < 0.5\,\mathrm{cm}$.

It is also important to note that we have no evidence that protonium has been formed via collisions with neutral H_2 molecules (for instance via the reactions $\overline{p} + H_2 \rightarrow \overline{p}p(n,l) + H^-$ and $\overline{p} + H_2 \rightarrow \overline{p}p(n,l) + H + e^-$). At the ambient temperature of the trap electrodes ($\sim 15\,\mathrm{K}$) the background pressure will be very low (typically less than $10^{-12}\,\mathrm{mbar}$) as evidenced by the very low residual annihilation rates of trapped antiprotons and positrons. Were protonium to be formed in $\overline{p}$-H_2 collisions, signal would also appear close to $r = 0$ at larger values of $|z|$ (in the so-called lateral wells of the nested charged particle traps) and very few events are present here, as seen in figs. 4(c) and 6(c) and from table 1, where the relevant value of F_c for the HM case is consistent with zero. Such events could be due to antiprotons bouncing back-and-forth in these wells, or perhaps trapped there, and axially separated from the positron plasma, as a result of collisions (see, *e.g.*, [63]). That the number of such events is negligible, together with the localised nature of the protonium signal, suggests that we have only observed protonium formed in interactions with H_2^+ ions in this experiment.

3.2 Cross-sections and energetics

In [25] it was argued that the cross-sections for production of protonium via reaction (1) calculated by Sakimoto [64] could explain the observed yields. Typically, ATHENA observed around 100 protonium annihilations, for both CM and HM cases, for every 60 s $\overline{p}$ injection cycle. With a vertex recovery efficiency of around 50%, this amounts to a time-averaged rate of a few per second. This corresponds to a yield of about $2 \times 10^{-4}\,\mathrm{s}^{-1}$ per $\overline{p}$ into mixing, though as we note below, not all of the injected antiprotons overlapped with the e^+ plasma in all of the experimental conditions we have investigated.

It is not, however, straightforward to make detailed estimates of the expected yields. In the two cases, CM and HM, in which the protonium signals can be extracted with confidence from antihydrogen annihilations, the spatial distribution of the H_2^+ ions is quite different. This phenomenon is caused by the difference in the thermal equilibrium

state of the positron plasma with an admixture of ions. At low positron temperatures, the size of the centrifugal barrier (here 250–640 K) [54,55,58] caused by the global $\mathbf{E} \times \mathbf{B}$ rotation of the plasma (and ions) results in the latter becoming separated from the positrons and forming, as discussed above, a narrow band near the equator of the plasma. Under HM conditions the thermal energy is sufficient to overcome this barrier, such that the ions will be distributed uniformly throughout the plasma.

Here we will only treat the HM case, since the increase in the positron temperature can be used to provide an estimate of the collision energy, and the number of ions per unit volume of the positron plasma can be calculated. The plasma parameters, z_p and r_p were deduced using non-destructive methods [39,40], assuming the plasma forms a spheroid of volume $4\pi r_p^3 \alpha/3$, where $\alpha = z_p/r_p$. Inserting typical values of $z_p = 1.6\,\mathrm{cm}$ and $r_p = 0.1\,\mathrm{cm}$, we find that the volume occupied by the ions is around $7 \times 10^{-8}\,\mathrm{m}^3$. Given that there are around 10^4 H_2^+ ions, the ionic density is thus about $1.5 \times 10^{11}\,\mathrm{m}^{-3}$.

The plasma temperature of 10000 K corresponds, assuming thermal equilibrium, to a kinetic energy of around 1 eV. We will use this as a rough estimate of the kinetic energy of the collision. Although Sakimoto's calculations [64] do not extend to below 2 eV, he has shown that the cross-section for reaction (1), $\sigma_{\overline{p}p}$, is proportional to the impact kinetic energy as E^{-1} at low energies (below about 5 eV). (Note that Sakimoto's results are in excellent accord with the later theoretical work of Cohen [65].) Thus, with $\sigma_{\overline{p}p} E \sim 8 \times 10^{-19}\,\mathrm{m}^2\,\mathrm{eV}$, a collision rate, per $\overline{p}$, can be found to be around $1.7 \times 10^{-3}\,\mathrm{s}^{-1}$ using a velocity of $1.4 \times 10^4\,\mathrm{ms}^{-1}$. With around 10^4 $\overline{p}$ also present in the trap, this gives a yield of about $17\,\mathrm{s}^{-1}$, and in excess of the observed value. However, due to the nature of the mixing in the nested trap, the antiprotons are not inside the positron plasma throughout the entire mixing time. Indeed, some antiprotons at large radii may not overlap the plasma at all, such that the realistic interaction rate will be lower than the simple estimate given above. If it is assumed that the entire depression of the yield is caused by the radial geometrical mismatch of the positron and antiproton clouds then, for circular cloud profiles, the antiprotons need only be around three times the size of the positrons (*i.e.*, about 3 mm in radius) to explain the difference between the observation and the estimate from theory. Furthermore, the antiproton thermalisation following injection into a 10000 K positron plasma is lengthened over that for the CM case, and may occupy a significant fraction of the mixing cycle. (The cooling time constant is proportional to $T_e^{3/2}$ which results in a factor of at least 10^3 between the CM and HM cases, with the period being of the order of 10 s in the latter case.) Thus, epithermal interactions may be important, and would further reduce the protonium yield.

It should also be noted that Sakimoto [64] gave some values for $\sigma_{\overline{p}p}$ for excited vibrational and rotational states, down to about 3 eV. It is likely that there would be a distribution of excited states in the 10000 K plasma. Making a reasonable extrapolation of Sakimoto's work to lower energies, it is likely that the cross-section will be about a factor of 2–3 larger than that used in the estimate above.

Assuming that the recoil energy of the protonium is zero (see the discussion in [25]), then the transfer of the proton is most likely to occur into a state at which the binding energy in the protonium is equal to the binding energy of the H_2^+ ion with respect to dissociation into $(H + p)$. The latter is around 2.6 eV, which leads to an estimate of the principal quantum number of the protonium, n, as $n = (13.6 \times 919/2.6)^{1/2} \sim 68$. As pointed out in [25], this is not in accord with the calculation of Sakimoto [64] who finds production peaked around $n = 34$, in the presence of substantial protonium recoil. Cohen [65] has a similar finding. Thus, further theoretical work in this area is motivated.

3.3 Effects of electron loading

As described in sect. 2, one of ATHENA's methods of loading its cooling electrons involved passing an e-current through the positron plasma. Subsequently it was found that positron-antiproton mixing with this method of electron loading resulted, as presented in figs. 4, 5 and 6 and the accompanying discussion, in annihilation distributions characteristic of a pure antihydrogen signal. Thus, it would appear that the H_2^+ ions have either been destroyed by the electrons prior to mixing or have been removed to a position in the trap where they do not overlap with the antiprotons.

Any process which results in the removal of H_2^+ ions by the electrons, even if, for instance, the result is a trapped proton, will lead to the removal of the protonium signal. Clearly, a p-$\overline{p}$ reaction, in the absence of a third body cannot result in protonium formation. Several electron collision processes can destroy H_2^+, and they have been investigated experimentally some time ago, by Mathur *et al.* [66], but particularly by Peart and Dolder [67–72]. This, and other related work has been reviewed by Tawara *et al.* [73]. The main processes are referred to as dissociative excitation ($e^- + H_2^+ \rightarrow e^- + p + H$) and, dominant below a collision kinetic energy of 1 eV, dissociative recombination ($e^- + H_2^+ \rightarrow H + H^*$).

The cross-sections for these reactions vary steeply with energy, rising above $10^{-19}\,\mathrm{m}^2$ below 1 eV. However, Tawara *et al.* [73] have pointed out that, due to the details of the sources used to produce the ions, the experimental data contain contributions from vibrationally excited states. With supporting theory [74], Tawara *et al.* have noted that the cross-sections for ground state H_2^+ may be lower by an order of magnitude. (It is unlikely, though, that excited vibrational states are present in our ETP experiments with the positron plasma temperature expected to be near the ambient of 15 K.)

Thus, we can only make a crude estimate of the likelihood of H_2^+ destruction by the traversing electron beam. The beam was pulsed on, to match the positron loading, for ten periods each of 500 μs, at a current of 10 μA. Thus, only around 3×10^{11} e^- crossed the H_2^+ ions. Using a generous cross-section estimate of $10^{-19}\,m^2$, and an H_2^+ ion density of $1.5 \times 10^{11}\,m^{-3}$ (see sect. 3.2, though, strictly, this applies only to the HM case) over a length of only a few mm, it can easily be seen that only around 10–100 ions would be removed by this flux. Thus, it is unlikely that electron collisions could completely remove the ions.

However, as mentioned above, it was noted that following the transmission of the electrons through the positron plasma, the density was reduced by a factor of 5–10, and this occurred mostly as a result of radial expansion. Following the work of Greaves and co-workers [75,76] this will have been accompanied by an increase in the plasma temperature, though, in the 3 T magnetic field, this excess would have radiated away within 1 second. The timescale of the expansion is likely to have been of the order of the inverse of the plasma frequency, $1/\nu_p = 2\pi(\sqrt{m\epsilon_0/n_e e^2}) \sim 5$ ns [75,76] for typical ATHENA conditions, which is much shorter than the electron pulse duration. Using the recent experience of the ALPHA antihydrogen collaboration on sympathetic compression of antiproton clouds [77] using the rotating electric field technique (see, *e.g.*, [78–80]) to compress electron clouds would suggest that the H_2^+ ions would not have time to react to the expansion of the positrons. (ALPHA found that if they compressed their electron plasmas too quickly, in times of order 1 second, the antiproton cloud remained at its original size.) Thus, the H_2^+ ions will find themselves immersed in a less dense plasma whose rotation frequency, which is directly proportional to n_e, was suddenly lower than that of the ions. This would cause a negative torque and force the ions to expand in a manner similar to that found when rotating fields are applied to plasmas at lower frequencies than that of their natural rotation [81–83]. Thus, the ions may be lost from the trap, or moved out sufficiently far from the axis that they no longer interact with the antiproton cloud. This last possibility is in agreement with the observations of Andresen *et al.* [59], that have shown that the antiproton cloud is centrifugally separated from the electron one; in the present case when the positrons expand due to the electron interaction, the radius of the ion cloud should increase by a factor of 2–3 and the edge length up to a factor 10.The ions are thus spread over a larger volume of space and will have lower density near the plasma edge, where antiprotons tend to accumulate, reducing the protonium yield.

4 Conclusions

An experiment to form protonium via $\overline{p}$-H_2^+ interactions in vacuum has been described. We find formation rates of around $2 \times 10^{-4}\,s^{-1}$ per trapped $\overline{p}$, in reasonable accord with the estimates made using cross-section calculations of Sakimoto and Cohen. The protonium is formed at very low energies, and in states with annihilation lifetimes in the region of 1 μs. The experiment was performed with only 10^4–10^5 trapped ions, which were serendipitously introduced during positron transfer procedures for ATHENA's antihydrogen experiments. Dedicated studies, with purposely loaded ion clouds, could provide protonium yields several orders of magnitude higher than that recorded here, providing samples of a unique bound state system for further study.

We are grateful for support from a number of national funding agencies for the work of ATHENA including: EPSRC and The Royal Society (UK), INFN (Italy), MEXT (Japan) and SNF (Switzerland).

References

1. C.G. Parthey *et al.*, Phys. Rev. Lett. **107**, 203001 (2011).
2. L. Essen, R. Donaldson, M.J. Bangham, E.G. Hope, Nature **229**, 110 (1971).
3. K. Pachucki, D. Leibfried, M. Weitz, A. Huber, W. König, T.W. Hänsch, J. Phys. B: At. Mol. Opt. Phys. **29**, 177 (1996).
4. R. Pohl *et al.*, Nature **466**, 213 (2010).
5. M. Amoretti *et al.*, Nature **419**, 456 (2002).
6. G. Gabrielse *et al.*, Phys. Rev. Lett. **89**, 213401 (2002).
7. G.B. Andresen *et al.*, Nature **468**, 673 (2010).
8. G.B. Andresen *et al.*, Nature Phys. **7**, 558 (2011).
9. G.B. Andresen *et al.*, Phys. Lett. B **695**, 95 (2011).
10. G. Gabrielse *et al.*, Phys. Rev. Lett. **108**, 113002 (2012).
11. C. Amole *et al.*, Nature **483**, 439 (2012).
12. Y. Enomoto *et al.*, Phys. Rev. Lett. **105**, 243401 (2010).

13. M.S. Fee, A.P. Mills Jr., S. Chu, E.D. Shaw, K. Danzmann, R.J. Chichester, D.M. Zuckerman, Phys. Rev. Lett. **70**, 1397 (1993).
14. M.S. Fee, S. Chu, A.P. Mills Jr., R.J. Chichester, D.M. Zuckerman, E.D. Shaw, K. Danzmann, Phys. Rev. A **48**, 192 (1993).
15. S. Chu, A.P. Mills Jr., A.G. Yodh, K. Nagamine, Y. Miyake, T. Kuga, Phys. Rev. Lett. **60**, 101 (1988).
16. F.E. Maas *et al.*, Phys. Lett. A **187**, 247 (1994).
17. V. Meyer *et al.*, Phys. Rev. Lett. **84**, 1136 (2000).
18. T. Yamazaki, N. Morita, R.S. Hayano, E. Widmann, J. Eades, Phys. Rep. **366**, 183 (2002).
19. R.S. Hayano, M. Hori, D. Horváth, E. Widmann, Rep. Prog. Phys. **70**, 1995 (2007).
20. M. Hori *et al.*, Nature **475**, 484 (2011).
21. C.J. Batty, Rep. Prog. Phys. **52**, 1165 (1989).
22. D. Gotta, in *Low Energy Antiproton Physics*, edited by G. Kernel, P. Križan, M. Mikuž (World Scientific, 1995) p. 525.
23. A. Adamo *et al.*, Phys. Lett. B **285**, 15 (1992).
24. A. Bianconi *et al.*, Phys. Lett. B **487**, 224 (2000).
25. N. Zurlo *et al.*, Phys. Rev. Lett. **97**, 153401 (2006).
26. M. Hori, A. Dax, J. Eades, K. Gomikawa, R.S. Hayano, N. Ono, W. Pirkl, E. Widmann, H.A. Torii, B. Juhász, D. Barna, D. Horváth, Phys. Rev. Lett. **96**, 243401 (2006).
27. M. Amoretti *et al.*, Nucl. Instrum. Methods Phys. Res. A **518**, 679 (2004).
28. G. Gabrielse, X. Fei, K. Helmerson, S.L. Rolston, R. Tjoekler, T.A. Trainor, H. Kalinowsky, J. Haas, W. Kells, Phys. Rev. Lett. **57**, 2504 (1986).
29. G. Gabrielse, X. Fei, L.A. Orozco, R. Tjoekler, J. Haas, H. Kalinowsky, T.A. Trainor, W. Kells, Phys. Rev. Lett. **63**, 1360 (1989).
30. X. Feng, M.H. Holzscheiter, M. Charlton, J. Hangst, N.S.P. King, R.A. Lewis, J. Rochet, Y. Yamazaki, Hyperfine Interact. **109**, 145 (1997).
31. P.J. Schultz, K.G. Lynn, Rev. Mod. Phys. **60**, 701 (1988).
32. A.P. Mills Jr., E.M. Gullikson, Appl. Phys. Lett. **49**, 1121 (1986).
33. R. Khatri, M. Charlton, P. Sferlazzo, K.G. Lynn, A.P. Mills Jr., L.O. Roellig, Appl. Phys. Lett. **57**, 2374 (1990).
34. R.G. Greaves, C.M. Surko, Can. J. Phys. **74**, 445 (1996).
35. C.M. Surko, M. Leventhal, A. Passner, Phys. Rev. Lett. **62**, 901 (1989).
36. T.J. Murphy, C.M. Surko, Phys. Rev. A **46**, 5696 (1992).
37. D.P. van der Werf, L.V. Jørgensen, T.L. Watson, M. Charlton, M.J.T. Collier, M. Doser, R. Funakoshi, Appl. Surf. Sci. **194**, 312 (2002).
38. L.V. Jørgensen *et al.*, Phys. Rev. Lett. **95**, 025002 (2005).
39. M. Amoretti *et al.*, Phys. Rev. Lett. **91**, 055001 (2003).
40. M. Amoretti *et al.*, Phys. Plasmas **10**, 3056 (2003).
41. D.H.E. Dubin, Phys. Rev. Lett. **66**, 2076 (1991).
42. D.H.E. Dubin, Phys. Fluids B **5**, 295 (1993).
43. M. Amoretti *et al.*, Phys. Lett. B **578**, 23 (2004).
44. L.S. Fornari, L.M. Diana, P.G. Coleman, Phys. Rev. Lett. **51**, 2276 (1983).
45. D. Fromme, G. Kruse, W. Raith, G. Sinapius, J. Phys. B: At. Mol. Opt. Phys. **21**, L262 (1988).
46. J. Moxom, G. Laricchia, M. Charlton, J. Phys. B: At. Mol. Opt. Phys. **26**, L367 (1993).
47. G. Gabrielse *et al.*, Phys. Lett. B **455**, 311 (1999).
48. C. Regenfus, Nucl. Instrum. Methods Phys. Res. A **501**, 65 (2003).
49. N. Madsen *et al.*, Phys. Rev. Lett. **94**, 033403 (2005).
50. R. Armenteros, B. French, in *Antinucleon-nucleon Interactions in High Energy Physics*, edited by E.H.S. Burhop, Vol. **4** (Academic Press, New York, 1996) p. 237.
51. M. Fujiwara *et al.*, Phys. Rev. Lett. **92**, 065005 (2004).
52. E. Butler, *Antihydrogen formation, dynamics and trapping*, unpublished thesis (Swansea University, 2011).
53. M.H. Holzscheiter, M. Charlton, M.M. Nieto, Phys. Rep. **402**, 1 (2004).
54. T.M. O'Neil, Phys. Fluids **24**, 447 (1981).
55. D.H.E. Dubin, T.M. O'Neil, Rev. Mod. Phys. **71**, 87 (1999).
56. H. Imajo, K. Hayasaka, R. Ohmukai, U. Tanaka, M. Watanabe, S. Urabe, Phys. Rev. A **55**, 1276 (1997).
57. L. Gruber, J.P. Holder, J. Steiger, B.R. Beck, H.E. DeWitt, J. Glassman, J.W. McDonald, D.A. Church, D. Schneider, Phys. Rev. Lett. **86**, 636 (2001).
58. B.M. Jelenković, A.S. Newbury, J.J. Bollinger, W. Itano, T.B. Mitchell, Phys. Rev. A **67**, 063406 (2003).
59. G.B. Andresen *et al.*, Phys. Rev. Lett. **106**, 145001 (2011).
60. G. Gabrielse *et al.*, Phys. Rev. Lett. **105**, 213002 (2010).
61. S. Jonsell, D.P. van der Werf, M. Charlton, F. Robicheaux, J. Phys. B: At. Mol. Opt. Phys. **42**, 215002 (2009).
62. G.B. Andresen *et al.*, Phys. Lett. B **685**, 141 (2010).
63. M. Amoretti *et al.*, Phys. Lett. B **590**, 133 (2004).
64. K. Sakimoto, J. Phys. B: At. Mol. Opt. Phys. **37**, 2255 (2004).
65. J.S. Cohen, J. Phys. B: At. Mol. Opt. Phys. **38**, 441 (2005).
66. D. Mathur, S.U. Khan, J.B. Hasted, J. Phys. B: At. Mol. Phys. **11**, 3615 (1978).
67. B. Peart, K.T. Dolder, J. Phys. B: At. Mol. Phys. **4**, 1496 (1971).

68. B. Peart, K.T. Dolder, J. Phys. B: At. Mol. Phys. **5**, 860 (1972).
69. B. Peart, K.T. Dolder, J. Phys. B: At. Mol. Phys. **5**, 1554 (1972).
70. B. Peart, K.T. Dolder, J. Phys. B: At. Mol. Phys. **6**, 2409 (1973).
71. B. Peart, K.T. Dolder, J. Phys. B: At. Mol. Phys. **7**, 236 (1974).
72. B. Peart, K.T. Dolder, J. Phys. B: At. Mol. Phys. **8**, 1570 (1975).
73. H. Tawara, Y. Itikawa, H. Nishimura, M. Yoshino, J. Chem. Phys. Ref. Data **19**, 617 (1990).
74. C. Bottcher, J. Phys. B: At. Mol. Phys. **9**, 2899 (1976).
75. G.P. Zank, R.G. Greaves, Phys. Rev. E **51**, 6079 (1995).
76. R.G. Greaves, C.M. Surko, Phys. Rev. Lett. **75**, 3846 (1995).
77. G.B. Andresen *et al.*, Phys. Rev. Lett. **100**, 203401 (2008).
78. F. Anderegg, E.M. Hollmann, C.F. Driscoll, Phys. Rev. Lett. **81**, 4875 (1998).
79. R.G. Greaves, C.M. Surko, Phys. Rev. Lett. **85**, 1883 (2000).
80. J.R. Danielson, C.M. Surko, Phys. Rev. Lett. **94**, 035001 (2005).
81. E.M. Hollman, F. Anderegg, C.F. Driscoll, Phys. Plasmas **7**, 2776 (2000).
82. R.G. Greaves, C.M. Surko, Phys. Plasmas **8**, 1879 (2001).
83. J.R. Danielson, C.M. Surko, T.M. O'Neil, Phys. Rev. Lett. **99**, 135005 (2007).